Check for updates

Rational design of ZnO@ZIF-8 nanoarrays for improved electrochemical detection of H_2O_2

Houshan Mei, Jiayue Xie, Zishuo Li, Chengming Lou, Guanglu Lei, Xianghong Liu [ID] and Jun Zhang [ID] *

Metal oxide nanostructures hold great promise in biosensors for non-enzymatic detection of H_2O_2. However, the interfacial or morphological changes of metal oxides during electrochemical reactions due to corrosion greatly reduce the service life and stability of the sensor. In this work, we propose the utilization of zeolite imidazole framework-8 (ZIF-8) as a functional layer to improve the H_2O_2 detection properties of ZnO nanorod arrays. Benefiting from the synergic interaction of the two materials, the core–shell ZnO@ZIF-8 nanoarrays demonstrate significantly enhanced electrochemical performance compared to pristine ZnO, delivering a wider linear range (20–11 550 μM) at 0.6 V potential, higher sensitivity (4.47 μA mM^{-1} cm^{-2}) and low detection limit (3 μM), as well as appealing long-term stability of up to 21 days. Post-TEM analysis reveals that the ZIF-8 shells can effectively protect the ZnO cores from corrosion when immersed in electrolyte to detect H_2O_2. The core–shell structure formed by coating metal–organic frameworks on metal oxides provides a new pathway for high performance chemical detection and other related fields.

1. Introduction

In recent years, detection of hydrogen peroxide (H_2O_2) has attracted significant attention because of its important role in food, agriculture, medicine and health, clinical control and environmental monitoring.[1,2] Excess H_2O_2 produced by human metabolism can cause a series of central nervous system diseases and seriously harm people's health.[3] At the same time, the formation of acid rain in nature is also connected to the formation of H_2O_2. Therefore, it is particularly important to develop a fast, efficient and stable H_2O_2 sensor. Among the various methods currently proposed for detecting H_2O_2, the electrochemical detection of H_2O_2 has become the simplest and most effective one due to its high sensitivity, low cost, and low power consumption.[4]

Due to their high surface-to-volume ratio, abundant molecular adsorption sites and high carrier mobility, one-dimensional (1D) metal oxide nanostructures such as nanowires and nanorods have demonstrated great potential in nanodevices, especially in the field of chemical sensors.[5–8] Manipulating 1D units into three-dimensional (3D) nanoarray structures further enhances their application potential in chemical sensors.[7,9,10] These 3D nanoarray structures can greatly improve the adsorption, reaction and diffusion of

molecules due to the abundant space between 1D building blocks, thereby exhibiting better sensing performance.[11]

ZnO nanostructures have been widely used as sensing materials for H_2O_2 biosensors. Liu *et al.* reported a simple and rapid hydrothermal method to grow ZnO nanorods on stainless steel foil as H_2O_2 sensors with a low detection limit of 0.27 μM and a linear range of 0.1–100 μM.[12] At the same time, Al-Hardan *et al.* reported a H_2O_2 sensor with ZnO nanorods grown on conductive glass as the sensing material. The prepared sensor has a linear range of 10–700 μM and a lower detection limit of 42 μM.[13] In addition, Li *et al.* prepared Au–ZnO composite nanofibers by electrospinning as the electrode material of the H_2O_2 sensor, which has a good linear relationship and sensitivity in the range of 1–6000 μM, and a lower detection limit of 0.1 μM.[14] Although the proposed H_2O_2 sensor based on the ZnO nanostructure has a wide linear range and a low detection limit, due to the inevitable agglomeration of ZnO used as a sensing material, the specific surface area and active center of the nanomaterial are reduced, thus reducing the service life and stability of the sensor. As a result, the current H_2O_2 sensor based on ZnO has difficulty maintaining a certain stability after 15 days. Therefore, there is an urgent need for a method to reduce or even avoid the corrosion and agglomeration of ZnO to improve the long-term stability and life of the sensor.

Due to their ordered structure, metal–organic frameworks (MOFs) as new multi-void crystalline materials have a large internal surface area.[15–17] Recently, MOFs have been used to

College of Physics, Center for Marine Observation and Communications, Qingdao University, Qingdao 266071, China. E-mail: jun@qdu.edu.cn

produce core–shell structures by encapsulating metal oxides.[18] The obtained metal oxide@MOF materials exhibit novel physical and chemical properties in various sensor applications because of the unique molecule-screening functions of the MOF shells.[19–21] As reported by Zhan et al.,[22] a simple self-templating method was used to successfully synthesize ZnO@ZIF-8 nanorods for the detection of H_2O_2 and ascorbic acid. In this process, ZnO nanorods not only serve as templates, but also provide Zn^{2+} ions for the formation of ZIF-8. As expected, due to the different molecular sizes of H_2O_2 and ascorbic acid and the pore size limitation of ZIF-8, the detection of H_2O_2 and ascorbic acid showed completely different current signals. Meanwhile, it has been reported that Cu-MOF and Mn-MOF composites were able to protect carbon steel from corrosion at 3.5 wt% NaCl solution.[23] It is noted that ZnO@zeolite imidazole framework-8 (ZnO@ZIF-8) core–shell materials have been frequently investigated as chemical gas sensors to selectively detect acetone[24–26] and formaldehyde,[27] while very rare attention has been paid to them as electrochemical sensors.[22]

In this work, we fabricate ZnO@ZIF-8 core–shell nanoarrays and explore their utilization in electrochemical sensors for H_2O_2 detection. Experiments show that the composite nanoarrays demonstrate high sensitivity and good linearity in a wide range of H_2O_2 concentrations. A very low detection limit of 3 μM has been obtained, which is 16-times lower than that of pristine ZnO. Meanwhile the ZnO@ZIF-8 sensor manifests excellent anti-interference ability against interfering molecules including dopamine (DA), ascorbic acid (AA), uric acid (UA), glucose (GO), lysine and NaCl in the electrolyte. Importantly, it is found that ZIF-8 layers also enable the sensor to have a long-term stability due to the protection of ZnO from corrosion as proved by post-TEM observation.

2. Experimental section

2.1 Chemicals

Zinc acetate, zinc nitrate hexahydrate, hexamethylenetetramine (HMT), N,N-dimethylformamide (DMF), and ethanol were purchased from Sinopharm Chemical Reagent Co. Polyethyleneimine (PEI) and 2-methylimidazole were purchased from Macleans. The phosphate buffer solution (PBS, 0.1 M) prepared by mixing sodium dihydrogen phosphate and sodium hydroxide solution and adjusted to the pH value of 7.0 is used as the supporting electrolyte for all test processes.

2.2 Fabrication of ZnO nanorod arrays

ZnO nanorod arrays were grown onto a glass substrate by a seed-assisted method following our previous work.[11] Firstly, ZnO seeds were deposited on the substrate. Typically, 40 μL 0.06 M zinc acetate solution was dropped onto 1×1 cm^2 ITO glass using a pipetting gun and dried at 80 °C. The obtained ITO was annealed at 350 °C for 30 min to prepare the seed layers. The ITO substrate was immersed in 80 mL of zinc nitrate hexahydrate (50 mM), HMT (60 mM) and PEI (3.6 mM) solution, and kept for 3 h at 90 °C, 8 h at 92.5 °C, 3 h at 95 °C, 4 h at 97.5 °C, 4 h at 105 °C, 2 h at 120 °C, and 2 h at
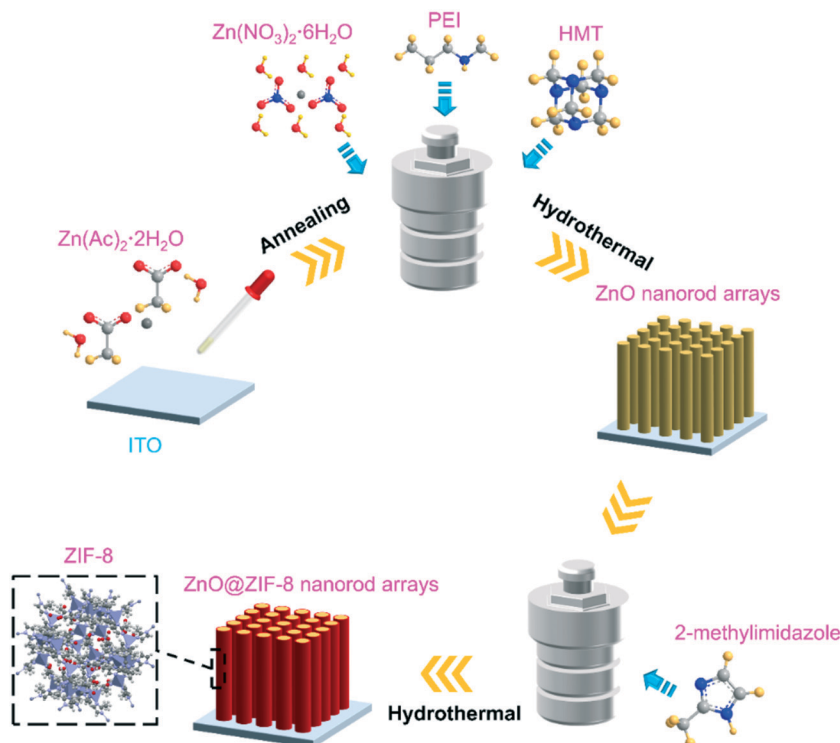

Fig. 1 Schematic illustration of the preparation of ZnO@ZIF-8 nanorod arrays.

130 °C. Finally, the ZnO nanorod arrays were washed with deionized water and dried at 80 °C.

2.3 Preparation of ZnO@ZIF-8 nanorod arrays

The ZnO@ZIF-8 nanorod arrays were synthesized by a hydrothermal method. Typically, ZnO nanorod arrays were immersed in 40 mL of DMF/H_2O (3 : 1 of v/v) mixed solution containing 2.5 mM 2-methylimidazole and kept in a Teflon-lined autoclave at 70 °C for 24 h. Finally, the ZnO@ZIF-8 nanorod arrays were washed with deionized water and dried at 70 °C.[22]

2.4 Characterization and electrochemical measurements

Under 200 kV pressure, ZnO and ZnO@ZIF-8 nanorods were observed using a transmission electron microscope (TEM) and a high resolution transmission electron microscope (HRTEM) on a JEM-2010. High-angle annular dark field scanning transmission electron microscopy (HAADF-STEM) and energy dispersive X-ray spectroscopy (EDX) elemental mapping were performed on an FEI Tecnai G20. Phase analysis was performed by powder X-ray diffraction (XRD). The surface composition of ZnO and ZnO@ZIF-8 was studied by X-ray photoelectron spectroscopy (XPS).

An electrochemical workstation (VSP, Bio-Logic) was used to record the cyclic voltammograms (CVs) of the sensor between 0 and 1.0 V (*vs.* Ag/AgCl) in 0.1 M PBS at 50 mV s^{-1}. For chronoamperometry, under magnetic stirring, the current response of the sensor was recorded with the continuous dripping of hydrogen peroxide. The applied potential was 0.6 V (*vs.* Ag/AgCl). All electrochemical tests were performed at room temperature. For Mott–Schottky measurement, ZnO and ZnO@ZIF-8 nanoarrays were used as the working electrodes, the platinum sheet as the counter electrode, and Ag/AgCl as the reference electrode in 1 M Na_2SO_4 electrolyte.
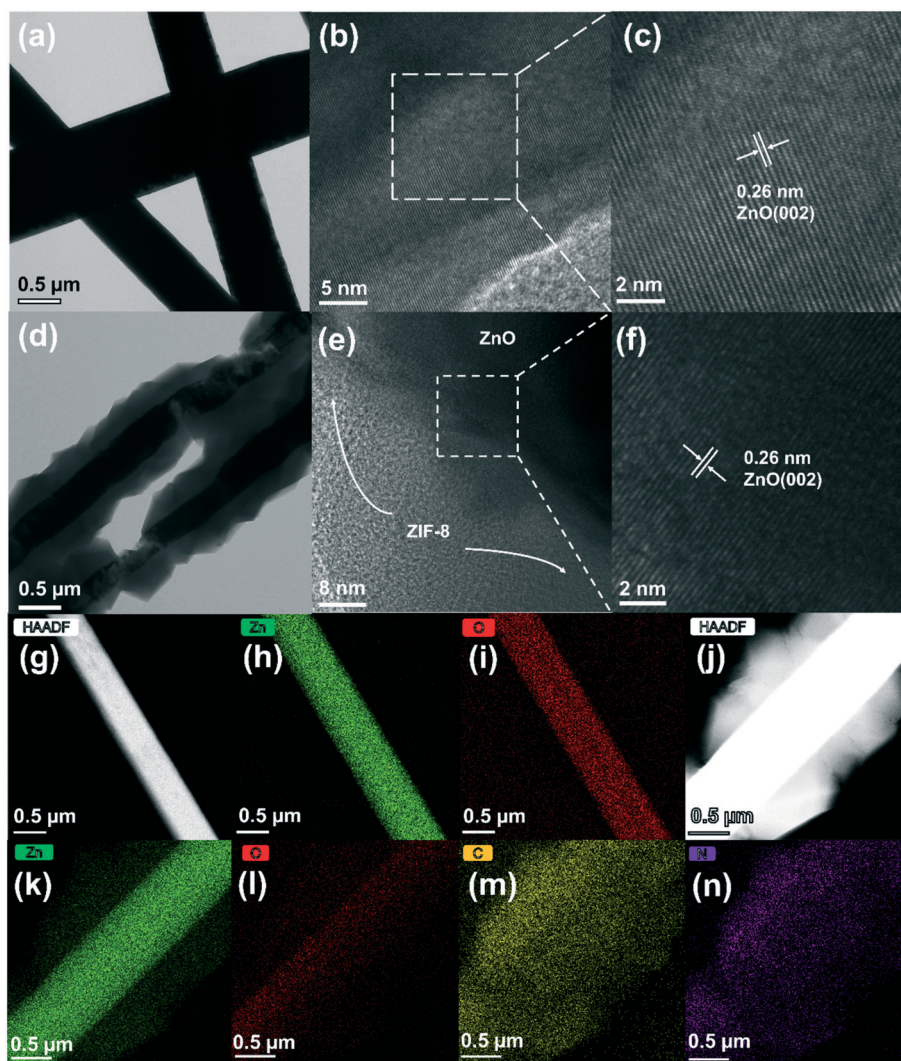

Fig. 2 TEM images of ZnO (a) and ZnO@ZIF-8 nanorods (d); HRTEM images of ZnO (b and c) and ZnO@ZIF-8 nanorods (e and f). The HAADF-STEM image with the corresponding mapping of ZnO (g–i) and ZnO@ZIF-8 nanorods (j–n).

3. Results and discussion

3.1 Morphological and structure characterization

The synthesis process of ZnO@ZIF-8 nanorod arrays is schematically shown in Fig. 1. The first step is to fabricate a zinc oxide seed layer on ITO. The second step is to synthesize ZnO nanorod arrays by a hydrothermal method. Then, ZnO nanorod arrays are converted into ZnO@ZIF-8 nanorod arrays by a hydrothermal method. Fig. 2(a and d) shows the TEM images of ZnO and ZnO@ZIF-8 nanorods. It can be observed that ZIF-8 is relatively completely coated on ZnO. Among them, the zinc oxide core of the ZnO@ZIF-8 nanorod is much thinner than the original ZnO nanorod. At the same time, Fig. 2 gives more details about the ZnO nanorod (b and c) and ZnO@ZIF-8 nanorod (e and f) through HRTEM. It can be observed from Fig. 2(c and f) that lattice fringes with a lattice spacing of 0.26 nm correspond to the (002) plane of zinc oxide.

The chemical elements of ZnO nanorods and ZnO@ZIF-8 nanorods were tested by HADDF-STEM and EDX. In Fig. 2(g–i), the elemental mapping images reveal the element distribution of Zn and O in ZnO nanorods. Fig. 2(j–n) also show the Zn, O, N and C elements in ZnO@ZIF-8 nanorods. The presence of N and C elements also reveals that ZIF-8 can be successfully transformed. It can be seen that ZIF-8 is well coated on ZnO nanorods, forming a core–shell structure of the ZnO@ZIF-8 nanorod. In addition, in Fig. 2(j), the ZnO nanorod as the core exhibits a brighter contrast than the ZnO@ZIF-8 nanorod due to its larger atomic mass.

Fig. 3 shows the XRD patterns of the ZnO nanorod and ZnO@ZIF-8 nanorod measured directly on ITO glass. It can be seen that the XRD patterns of the ZnO nanorod and ZnO@ZIF-8 nanorod are completely consistent with the wurtzite structure of zinc oxide (PDF#36-1451).[28] In addition, compared to the ZnO nanorod, the peak at 10 to 20° in the ZnO@ZIF-8 nanorod corresponds to the lattice structure of the newly generated ZIF-8. And after being coated with ZIF-8, the additional new peaks appearing are consistent with the published simulation spectrum of the ZIF-8 structure data. The superposition of each group of diffraction peaks in ZnO@ZIF-8 indicates that ZnO and ZIF-8 coexist in the obtained nanocomposite.[29]

The Mott–Schottky curves of ZnO and ZnO@ZIF-8 nanorods are shown in Fig. 4(a). Both curves show a positive slope,[30] indicating that both ZnO and ZnO@ZIF-8 nanorods exhibit n-type conductivity.[30]

XPS measurement was performed to determine the surface chemical states of ZnO and ZnO@ZIF-8 nanorods. As shown in Fig. 4(b), the survey scan of the ZnO@ZIF-8 nanorod shows Zn 2p, O 1s, N 1s, and C 1s, while only Zn 2p, O 1s and C 1s can be observed in the spectrum of ZnO. For the ZnO@ZIF-8 nanorod, the appearance of the N 1s peak and the enhancement of the C 1s peak indicate the successful synthesis of ZIF-8. For the two samples, the Zn 2p peaks of pure ZnO and ZnO@ZIF-8 are different. In ZnO, the peaks of the core-level spectrum of Zn 2p at 1044.24 eV and 1021.09 eV are attributed to Zn $2p_{1/2}$ and Zn $2p_{3/2}$.[11] For ZnO@ZIF-8, the peak for Zn $2p_{3/2}$ is deconvoluted into two peaks, which belong to Zn–N (1021.46 eV) and Zn–O
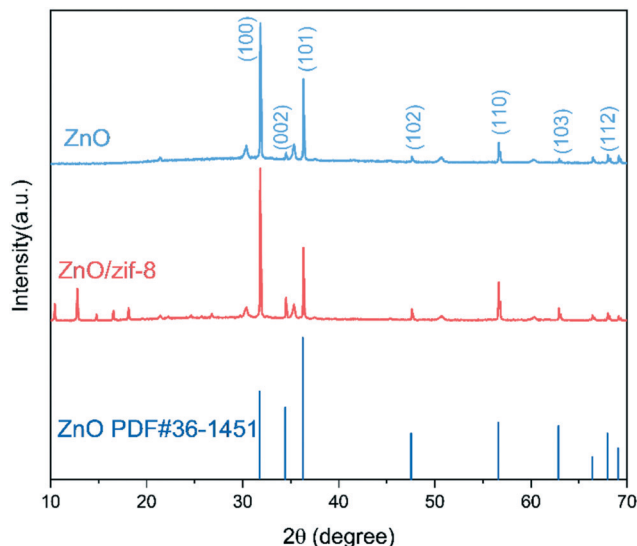

Fig. 3 The XRD patterns of the ZnO nanorod and ZnO@ZIF-8 nanorod.

(1022.89 eV) respectively.[31] In Fig. 4(c), the O 1s spectrum of ZnO can be fitted into three peaks at 532.24 eV, 530.89 eV and 529.69 eV, which are attributed to hydroxyl oxygen, adsorbed oxygen and lattice oxygen.[32–34] The O 1s spectra of ZnO@ZIF-8 respectively at 534.06 eV, 531.51 eV and 529.96 eV are attributed to hydroxyl oxygen, adsorbed oxygen and lattice oxygen.[8,29] Among them, due to the introduction of ZIF-8 with high specific surface area, ZnO@ZIF-8 (55.56%) has a much higher ratio of adsorbed oxygen than ZnO (48.83%). The N 1s fitting of ZnO@ZIF-8 has two peaks located at 400.86 eV and 398.76 eV, which belong to the N atom in the Zn–N bond and the N atom linked by imidazole (Fig. 4(e)).[29] In Fig. 4(f), the two fitting peaks at 285.96 eV and 284.56 eV in the C 1s spectrum of ZnO@ZIF-8 correspond to the sp² C bond in the heterocyclic ring N═C–N and the sp² hybridized C atom in the imidazole ring, respectively.[29]

3.2 Electrochemical detection of H₂O₂

Fig. 5(a) shows the electrochemical responses of different electrodes obtained by cyclic voltammetry (CV) in 0.1 M pH 7.0 PBS containing 1 mM H_2O_2. According to Li's report, since the impedance of the material increases after coating with ZIF-8, the current signal of ZnO is higher than that of ZnO@ZIF-8 at a lower potential.[35] However, at a higher potential, the ZnO@ZIF-8 nanorod array has a higher current signal than the ZnO nanorod array. This is mainly due to the porous structure and larger specific surface area of the ZIF-8 coating, which increases the adsorbed oxygen content of the material, so more H_2O_2 molecules participate in the redox reaction, thereby improving the current signal.[8] Fig. 5(b) shows the cyclic voltammetry curves of ZnO@ZIF-8 nanorods in 0.1 M pH 7.0 PBS containing different concentrations of H_2O_2. The current response of ZnO@ZIF-8 nanorod arrays increases with the increase of H_2O_2 concentration. Due to the porosity of ZIF-8, H_2O_2 can pass through without
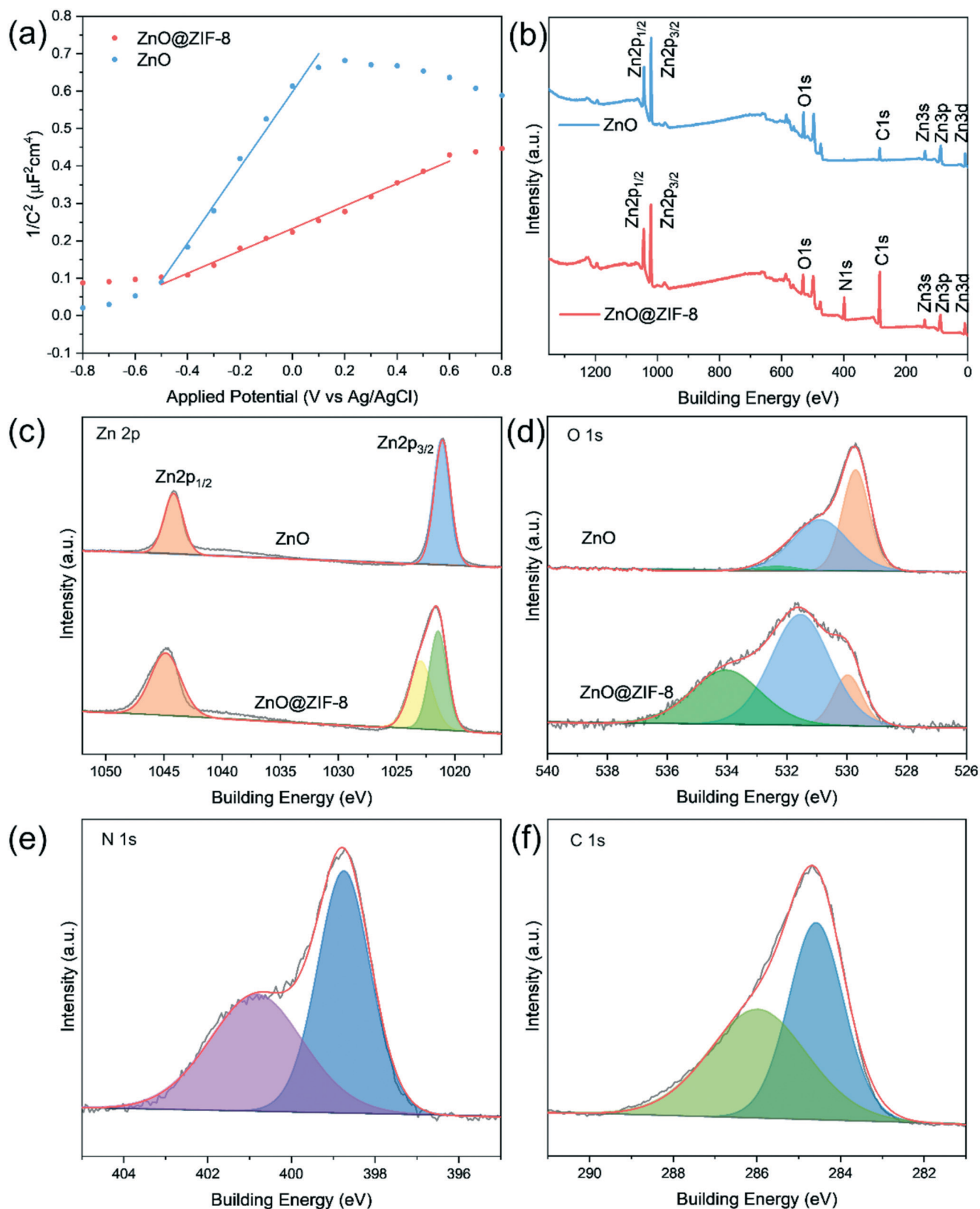
Fig. 4 (a) Mott–Schottky plots of the ZnO nanorod and ZnO@ZIF-8 nanorod. (b) XPS analysis of ZnO and ZnO@ZIF-8 nanorods, and high resolution spectra of Zn 2p (c), O 1s (d), N 1s (e) and C 1s (f).
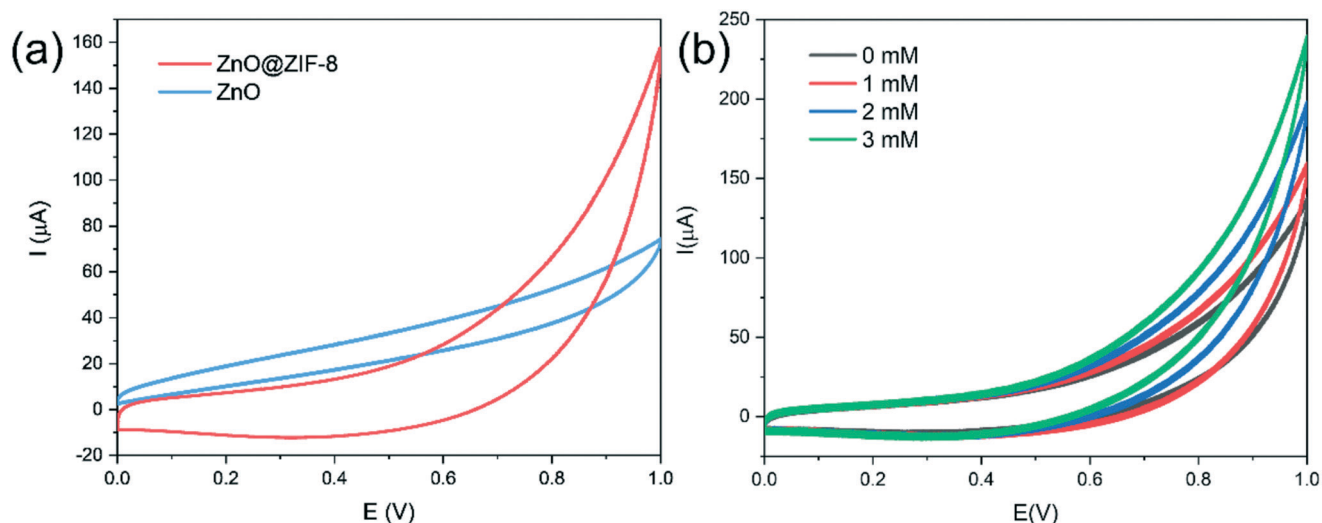
Fig. 5 (a) Cyclic voltammograms of the ZnO nanorod arrays and the ZnO@ZIF-8 nanorod arrays in the presence of 1 mM H_2O_2 in PBS (0.1 M, pH 7.0) at a scan rate of 50 mV s^{-1}; (b) cyclic voltammograms of ZnO@ZIF-8 nanorod arrays in PBS including various concentrations of H_2O_2 at 50 mV s^{-1}.

hindering diffusion. Therefore, ZnO@ZIF-8 has relatively good performance as a sensing material for detecting H_2O_2.

The fast and sensitive detection ability of ZnO and ZnO@ZIF-8 nanorod arrays for H_2O_2 was tested by the current response of continuously adding H_2O_2. As shown in Fig. 6, at a potential of 0.6 V, both ZnO and ZnO@ZIF-8 nanorod arrays show a clear current response to the addition of H_2O_2, and can reach 95% of the steady-state current value within 5 s. However, as shown in Fig. 6(b, d and f), after the long-term current response to the addition of H_2O_2, it is found that the current response and sensitivity of ZnO nanorod arrays continue to decrease, while the current response and sensitivity of ZnO@ZIF-8 nanorod arrays almost remain in a stable state. The sensitivity of ZnO nanorod arrays was 0.00599 μA μM^{-1} cm^{-2} on the first day, but after twenty one days, the sensitivity of the test dropped to 0.0008 μA μM^{-1} cm^{-2}. The sensitivity of ZnO@ZIF-8 nanorod arrays remains above 0.004 μA μM^{-1} cm^{-2}. A sensitivity of 0.00477 μA μM^{-1} cm^{-2} can be reached in the first test. The reason for the analysis may be due to ZnO nanorod arrays corroding after long-term testing, and ZnO@ZIF-8 nanorod arrays can maintain the stability of detecting H_2O_2 due to the protection of ZIF-8. By fitting the response current value in Fig. 6(e), the linear regression equations of ZnO nanorod arrays and ZnO@ZIF-8 nanorod arrays are I (μA) = 2.70 + 0.0008C (μM) and I (μA) = 5.64 + 0.0048C (μM), and the correlation coefficients (R^2) are 0.996 and 0.992, respectively. In addition, the result of the lower limit of detection (LOD) is based on the ratio of the standard deviation (SD) of the current response to the slope of the calibration curve at a signal-to-noise ratio (SNR) of 3:[36,37]
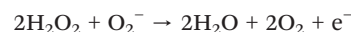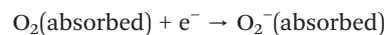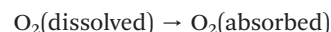
$$LOD = \frac{3SD}{S}$$

where SD is the standard deviation of the blank sample, and S is the sensitivity (the slope of the fitted straight line). In

Fig. 6(b, d and f), the long-term test results show that the lower detection limit of ZnO@ZIF-8 nanorod arrays remains at about 3 μM, but ZnO nanorod arrays have a higher detection limit of 50 μM due to the reduced sensitivity caused by more severe corrosion. In addition, the linear range of ZnO@ZIF-8 nanorod arrays for detecting H_2O_2 is 20–11 550 μM. Table 1 lists the performance comparison between the prepared sensor and some previously reported sensors for detecting H_2O_2. Compared with other H_2O_2 sensors, ZnO@ZIF-8 nanoarrays show excellent performance, with advantages in sensitivity, linear range, and detection limit.

3.3 The electrochemical detection mechanism of H_2O_2 on ZnO@ZIF-8 nanorods

The mechanism of ZnO@ZIF-8 nanorods for detecting hydrogen peroxide is shown in Fig. 7. With the continuous dropping of H_2O_2, the detection mechanism of ZnO@ZIF-8 nanorods can be understood by the following reaction:[13,49,50]

$$O_2(\text{dissolved}) \rightarrow O_2(\text{absorbed})$$

$$O_2(\text{absorbed}) + e^- \rightarrow O_2^-(\text{absorbed})$$

$$2H_2O_2 + O_2^- \rightarrow 2H_2O + 2O_2 + e^-$$

According to Fig. 7 and the above reactions, dissolved oxygen molecules are chemically adsorbed onto the surface of the nanorods by attracting the electrons in the conduction band to form ionized oxygen species, resulting in a decrease in the charge carrier density.[13,51] The chemically adsorbed oxygen species (O_2^-) will form an electron depletion layer and a high barrier near the surface area, resulting in an increase in the resistance of the materials. However, when H_2O_2
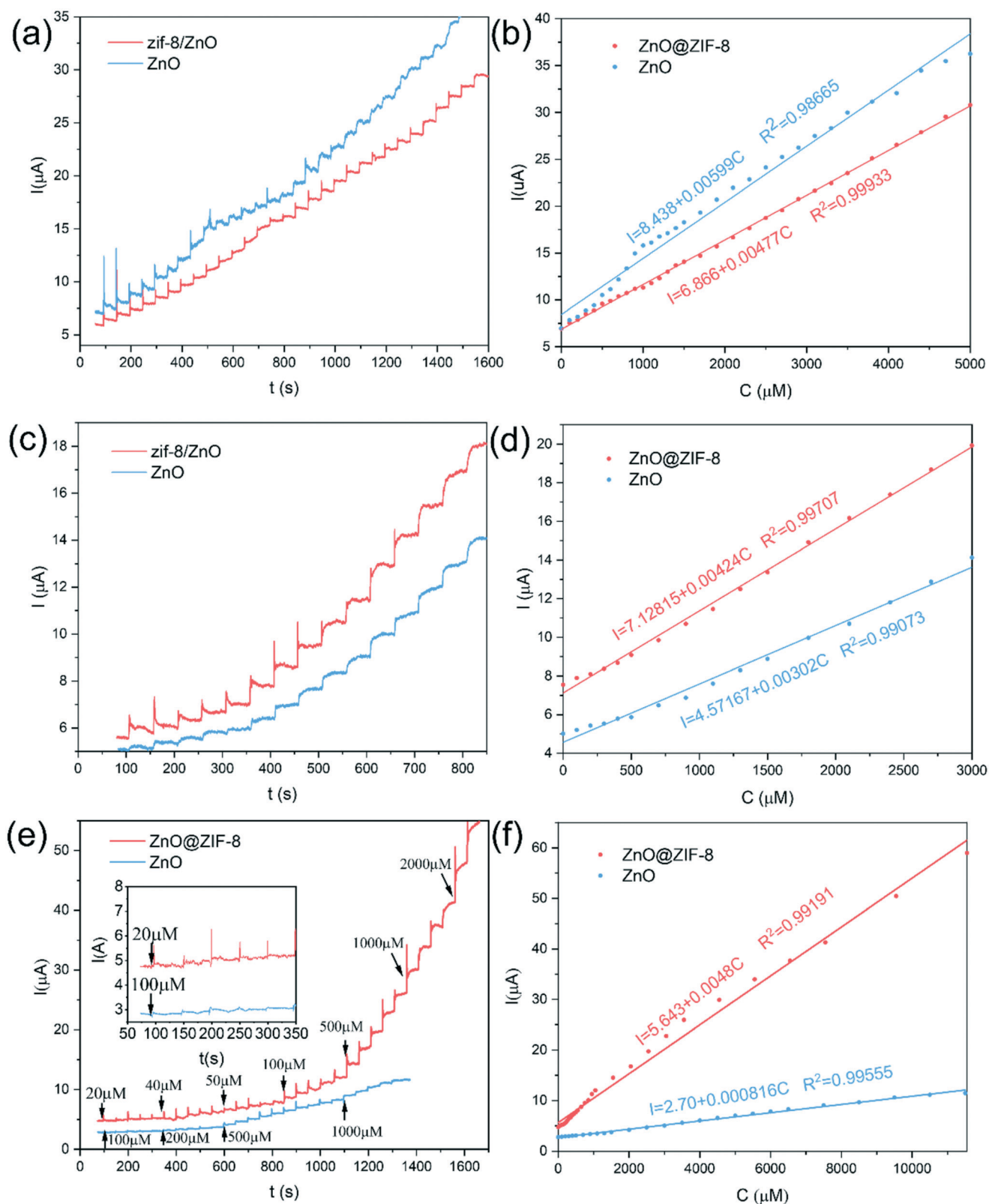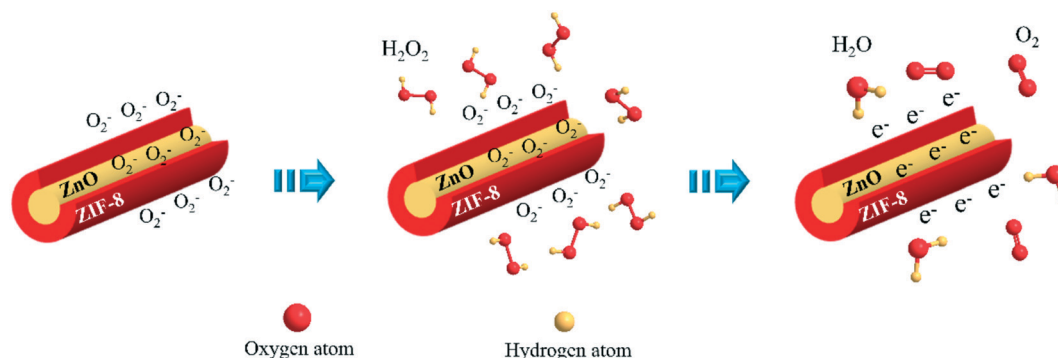
Fig. 6 The current response of ZnO and ZnO@ZIF-8 nanorod arrays to successive addition of H_2O_2 in PBS (0.1 M, pH 7.0) at an applied potential of 0.6 V on the first day (a and b), the seventh day (c and d) and the twenty-first day (e and f).

molecules are added to the electrolyte, the redox reaction between the H_2O_2 molecules and the oxygen adsorbed on the surface will release electrons to the sensing material, thereby reducing the electron depletion layer and potential barrier.[13]

Table 1 Performance comparison between ZnO@ZIF-8 nanorods and other H_2O_2 sensors

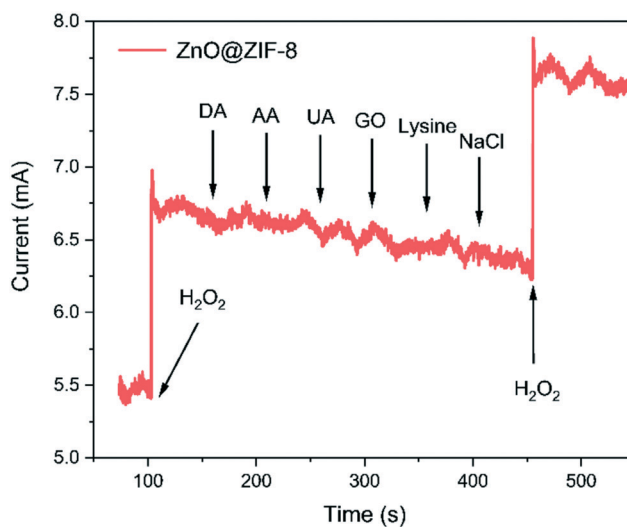| Materials	Linear range (μM)	Limit of detection (μM)	Sensitivity (μA mM^{-1} cm^{-2})
Cu$_2$O/rGO[38]	30–12 800	21.7	21.7 (μA mM^{-1})
ZnO nanorods[13]	10–700	42 to 143.5	2.95×10^{-4}
CuO–ZnO/FTO[39]	10–1000	9.998	0.357×10^{-3}
Ag–ZnO (ref. 40)	1–20	2.5	50.8×10^{-3}
n-CoZnO (ref. 41)	0.1–2400	11.1	13.3
Cu$_2$O/GNs[42]	300–7800	20.8	—
GNR-Fe$_3$O$_4$ (ref. 43)	0.5–7450	3.2	0.12
ZnO/CuO (ref. 44)	3–530	2.4	1.11×10^{-3}
Graphene/ZnO (ref. 45)	1–15 mM	7.4357	3.258 (μA mM^{-1})
Enzyme/ZnO (ref. 46)	4.8–200	2	—
ZnO-LIG5 (ref. 47)	0.8–14.6 mM	110	—
vG/NRs-F[48]	2–15 mM	320	39.6
ZnO@ZIF-8 (This work)	20–11 550	3	4.77

Fig. 7 Sensing mechanism of ZnO@ZIF-8 nanorod arrays.

Subsequently, due to the increase of electrons in the conduction band, the sensing material will assume a low resistance state, thereby increasing the current signal.[52] In the ZnO@ZIF-8 sensor, adsorbed oxygen can be regarded as a reactive oxygen species, which can act as an active center for unpaired electrons in ZnO@ZIF-8, resulting in more H_2O_2 molecules adsorbing onto the surface and facilitating subsequent redox reactions. In addition, due to the coating of ZIF-8, ZnO@ZIF-8 (55.56%) has more adsorbed oxygen than ZnO (48.83%), thus more H_2O_2 molecules can undergo redox reactions, which can increase the current signal more sensitively. Therefore, in the first chronoamperometry test, the high-impedance ZnO@ZIF-8 still has a sensitivity similar to that of the low-impedance ZnO at a lower potential of 0.6 V.

3.4 Selectivity and stability

As is known, many species such as AA, DA, UA and some carbohydrates will produce interference signals in the process of detecting H_2O_2, which makes the selectivity of H_2O_2 sensors a huge challenge.[15,53] As shown in Fig. 8, the anti-interference study of ZnO@ZIF-8 nanorod arrays is carried out by recording the current response of continuous injection of DA, AA, UA, GO, lysine and NaCl. Due to the suitable pore size and shape of ZIF-8, H_2O_2 molecules can pass through the ZIF-8 shell, but some larger molecules have difficulty passing through.[54] There is an obvious current response

Fig. 8 Amperometric response of ZnO@ZIF-8 nanorod arrays to the addition of 0.3 mM H_2O_2 or 0.1 mM other interferents in PBS (0.1 M, pH = 7.0) at an applied potential of 0.6 V.
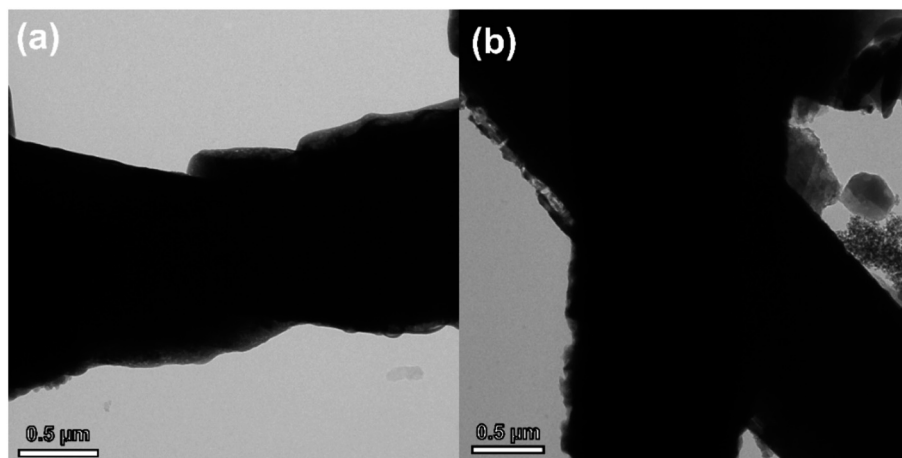
Fig. 9 TEM image of the ZnO nanorod (a) and ZnO@ZIF-8 nanorod (b) after the long-term test.

when H_2O_2 is dropped, but with continuous dropping of DA, AA, UA, GO, lysine and NaCl, no obvious current response is observed, and the relative error is less than ±15%. This shows that these interfering substances will not affect the detection of H_2O_2 by the prepared electrode materials.

In order to verify whether ZnO nanorods and ZnO@ZIF-8 nanorods are corroded during long-term H_2O_2 testing, we performed TEM on the ZnO nanorods and ZnO@ZIF-8 nanorods after H_2O_2 testing. As shown in Fig. 9(a), compared with the previously measured TEM image of the ZnO nanorod, after long-term detection of H_2O_2, the surface of the ZnO nanorod has been severely corroded. We infer that the ZnO nanorod reacts with H_2O_2 in the process of detecting H_2O_2 to generate Zn^{2+} ions that can be dissolved in the electrolyte. As a result, the specific surface area of the ZnO nanorod decreased, the available adsorption sites for H_2O_2 decreased, and the number of conduction centers decreased, which led to a decrease in the electrons responsible for conduction, thereby reducing the sensitivity of the sensor. At the same time, Lv's report shows that the presence of phosphate in PBS can significantly change the morphology of nano-zinc oxide, the surface of ZnO is significantly corroded, and nano-ZnO changes from ZnO to zinc phosphate over time.[55] However, in Fig. 9(b), it can be seen that there is almost no morphological change in the ZnO cores. This is because compared with ZnO nanorods, ZnO@ZIF-8 nanorods have a ZIF-8 shell and discrete Zn nodes. These Zn nodes will be oxidized by H_2O_2 from Zn^{1+} to Zn^{2+} to protect ZnO from reacting with H_2O_2.[56] Therefore, this may also be the cause of the partial dissolution of ZIF-8 as shown in Fig. 9(b). In addition, due to the selectivity of the ZIF-8 shell, the ZnO cores also avoided contact with phosphate. Therefore, the agglomeration and corrosion of the ZnO core are significantly reduced, and the performance of the sensor is greatly improved.

4. Conclusion

In summary, by designing a core–shell structure of ZnO@ZIF-8 nanoarrays, we clearly demonstrate the importance of MOF materials, i.e. ZIF-8, in protecting ZnO from surface corrosion to achieve extended stability in electrochemical sensors. Compared with the known H_2O_2 sensors, the excellent detection ability delivered by the ZnO@ZIF-8 nanoarrays have the following advantages: (i) the simplicity of the direct preparation method of ZnO@ZIF-8 nanoarrays by a hydrothermal method; (ii) the excellent stability and long life due to ZIF-8 coating to protect ZnO from corrosion; (iii) the excellent selectivity owing to the molecular sieving effect provided by ZIF-8. The results show that ZnO@ZIF-8 nanoarrays are promising electrochemical materials and may provide a new solution for constructing high-stability non-enzymatic electrochemical sensors.

Conflicts of interest

There are no conflicts to declare.

Acknowledgements

References

1 N. S. Lopa, M. M. Rahman, F. Ahmed, S. C. Sutradhar, T. Ryu and W. Kim, *Electrochim. Acta*, 2018, **274**, 49–56.

2 Q. Q. Jin, Z. L. Chen, Q. Chen, P. W. Yan, S. X. Zhao, J. M. Shen, L. Li, F. Guo and J. Kang, *J. Hazard. Mater.*, 2021, **404**, 124142.

3 J. Zhao, Y. L. Yan, L. Zhu, X. X. Li and G. X. Li, *Biosens. Bioelectron.*, 2013, **41**, 815–819.

4 N. Isoaho, E. Peltola, S. Sainio, J. Koskinen and T. Laurila, *RSC Adv.*, 2018, **8**, 35802–35812.

5 Z. Lou and G. Z. Shen, *Adv. Sci.*, 2016, **3**, 1500287.

6   T. T. Zhou, X. P. Liu, R. Zhang, Y. B. Wang and T. Zhang, *Sens. Actuators, B*, 2019, **290**, 210–216.

7   C. M. Lou, K. Wang, H. S. Mei, J. Y. Xie, W. Zheng, X. H. Liu and J. Zhang, *CrystEngComm*, 2021, **23**, 3654–3663.

8   Y. S. Xu, L. L. Zheng, C. Yang, W. Zheng, X. H. Liu and J. Zhang, *Sens. Actuators, B*, 2020, **310**, 127846.

9   N. Karimian and P. Ugo, *Curr. Opin. Electrochem.*, 2019, **16**, 106–116.

10 K. S. Ranjith, R. B. Castillo, M. Sillanpaa and R. T. R. Kumar, *Appl. Catal., B*, 2018, **237**, 128–139.

11 L. L. Zheng, J. Y. Xie, X. H. Liu, C. Yang, W. Zheng and J. Zhang, *ACS Appl. Mater. Interfaces*, 2020, **12**, 46267–46276.

12 W. Liu, W. T. Zhan, X. Y. Jia, Q. Liu, R. S. Chen, D. Li, Y. Huang, G. Y. Zhang and H. W. Ni, *Appl. Surf. Sci.*, 2019, **480**, 341–348.

13 N. H. Al-Hardan, M. A. Abdul Hamid, R. Shamsudin, N. K. Othman and L. Kar Keng, *Sensors*, 2016, **16**, 1044.

14 X. Li, G. D. Zhu, J. L. Dou, J. M. Yang, Y. X. Ge and J. Y. Liu, *Ionics*, 2019, **25**, 5527–5536.

15 S. L. Yang, N. Xia, M. Y. Li, P. P. Liu, Y. X. Wang and L. B. Qu, *RSC Adv.*, 2019, **9**, 15217–15223.

16 M. H. Yang, C. X. Duan, X. J. Zeng, J. J. Li, C. Y. Liu, L. J. Zeng, Y. Zhang, K. Wang and H. X. Xi, *Rare Met.*, 2021, **40**, 471–477.

17 J. Tang, Z. Z. Hui, T. Hu, X. Cheng, J. H. Guo, Z. R. Li and H. Yu, *Rare Met.*, 2022, **41**, 189–198.

18 H. L. Liu, L. N. Chang, C. H. Bai, L. Y. Chen, R. Luque and Y. W. Li, *Angew. Chem., Int. Ed.*, 2016, **55**, 5019–5023.

19 J. J. Zhou, P. Wang, C. X. Wang, Y. T. Goh, Z. Fang, P. B. Messersmith and H. W. Duan, *ACS Nano*, 2015, **9**, 6951–6960.

20 M. Saikia, D. Bhuyan and L. Saikia, *New J. Chem.*, 2015, **39**, 64–67.

21 B. K. Singh, S. Lee and K. Na, *Rare Met.*, 2020, **39**, 751–766.

22 W. W. Zhan, Q. Kuang, J. Z. Zhou, X. J. Kong, Z. X. Xie and L. S. Zheng, *J. Am. Chem. Soc.*, 2013, **135**, 1926–1933.

23 W. C. Wei, Z. Liu, R. Z. Wei, G. C. Han and C. X. Liang, *RSC Adv.*, 2020, **10**, 29923–29934.

24 M. S. Yao, W. X. Tang, G. E. Wang, B. Nath and G. Xu, *Adv. Mater.*, 2016, **28**, 5229–5234.

25 M. S. Yao, L. A. Cao, Y. X. Tang, G. E. Wang, R. H. Liu, P. N. Kumar, G. D. Wu, W. H. Deng, W. J. Hong and G. Xu, *J. Mater. Chem. A*, 2019, **7**, 18397–18403.

26 L. Tian, Y. X. Sun, H. L. Huang, X. Y. Guo, Z. H. Qiao, J. Q. Meng and C. L. Zhong, *ChemistrySelect*, 2020, **5**, 2401–2407.

27 H. L. Tian, H. Q. Fan, M. M. Li and L. T. Ma, *ACS Sens.*, 2016, **1**, 243–250.

28 Y. W. Li, Z. H. Tao, N. Luo, G. Sun, B. Zhang, H. H. Jin, H. Bala, J. L. Cao, Z. Y. Zhang and Y. Wang, *Sens. Actuators, B*, 2019, **290**, 607–615.

29 D. Tuncel and A. N. Okte, *Catal. Today*, 2021, **361**, 191–197.

30 Z. S. Li, X. H. Liu, M. Zhou, S. L. Zhang, S. Z. Cao, G. L. Lei, C. M. Lou and J. Zhang, *J. Hazard. Mater.*, 2021, **415**, 125757.

31 M. A. Haider, X. M. Yao, A. Loblaw and A. Finelli, *Can. Urol. Assoc. J.*, 2017, **11**, E1–E7.

32 L. J. Meng, C. P. Moreira de Sá and M. P. Dos Santos, *Appl. Surf. Sci.*, 1994, **78**, 57–61.

33 Z. S. Li, C. M. Lou, G. L. Lei, G. C. Lu, H. Y. Pan, X. H. Liu and J. Zhang, *Sens. Actuators, B*, 2022, **355**, 131347.

34 C. M. Lou, C. Yang, W. Zheng, X. H. Liu and J. Zhang, *Sens. Actuators, B*, 2021, **329**, 129218.

35 Y. Li, S. Xiao, W. Li, X. He, W. Fang, H. Chen, J. Ge and L. Zhao, *J. Mater. Sci.*, 2020, **55**, 7453–7463.

36 W. Zheng, C. Yang, Z. S. Li, J. Y. Xie, C. M. Lou, G. L. Lei, X. H. Liu and J. Zhang, *Sens. Actuators, B*, 2021, **329**, 129127.

37 Y. S. Xu, W. Zheng, X. H. Liu, L. Q. Zhang, L. L. Zheng, C. Yang, N. Pinna and J. Zhang, *Mater. Horiz.*, 2020, **7**, 1519–1527.

38 F. G. Xu, M. Deng, G. Y. Li, S. H. Chen and L. Wang, *Electrochim. Acta*, 2013, **88**, 59–65.

39 S. Chabri, A. Dhara, B. Show, D. Adak, A. Sinha and N. Mukherjee, *Catal. Sci. Technol.*, 2016, **6**, 3238–3252.

40 M. Hussain, H. Sun, S. Karim, A. Nisar, M. Khan, A. U. Haq, M. Iqbal and M. Ahmad, *J. Nanopart. Res.*, 2016, **18**, 95.

41 L. Wang, T. Wu, H. Wu, J. Zhong, N. Wang and R. M. Wang, *Prog. Nat. Sci.: Mater. Int.*, 2018, **28**, 24–27.

42 M. M. Liu, R. Liu and W. Chen, *Biosens. Bioelectron.*, 2013, **45**, 206–212.

43 A. M. Munshi, D. W. Ho, M. Saunders, V. Agarwal, C. L. Raston and K. S. Iyer, *Sens. Actuators, B*, 2016, **235**, 492–497.

44 S. Daemi, S. Ghasemi and A. A. Ashkarran, *J. Colloid Interface Sci.*, 2019, **550**, 180–189.

45 S. S. Low, M. T. T. Tan, H. S. Loh, P. S. Khiew and W. S. Chiu, *Anal. Chim. Acta*, 2016, **903**, 131–141.

46 G. Zhao, J. J. Xu and H. Y. Chen, *Anal. Biochem.*, 2006, **350**, 145–150.

47 J. Zanoni, J. P. Moura, N. F. Santos, A. F. Carvalho, A. J. S. Fernandes, T. Monteiro, F. M. Costa, S. O. Pereira and J. Rodrigues, *Chemosensors*, 2021, **9**, 102.

48 T. Hang, S. Xiao, C. Yang, X. L. Li, C. Guo, G. He, B. H. Li, C. D. Yang, H. J. Chen, F. M. Liu, S. Z. Deng, Y. Zhang and X. Xie, *Sens. Actuators, B*, 2019, **289**, 15–23.

49 C. Yang, L. W. Hu, H. Y. Zhu, Y. Ling, J. H. Tao and C. X. Xu, *J. Mater. Chem. B*, 2015, **3**, 2651–2659.

50 Y. Cheng, R. Yuan, Y. Chai, H. Niu, Y. Cao, H. Liu, L. Bai and Y. Yuan, *Anal. Chim. Acta*, 2012, **745**, 137–142.

51 M. M. Rahman and A. M. Asiri, *RSC Adv.*, 2015, **5**, 63252–63263.

52 Y. S. Xu, L. L. Zheng, C. Yang, X. H. Liu and J. Zhang, *Sens. Actuators, B*, 2020, **304**, 127237.

53 W. Gao, W. W. Tjiu, J. C. Wei and T. X. Liu, *Talanta*, 2014, **120**, 484–490.

54 J. Yang, H. L. Ye, F. Q. Zhao and B. Z. Zeng, *ACS Appl. Mater. Interfaces*, 2016, **8**, 20407–20414.

55 J. T. Lv, S. Z. Zhang, S. S. Wang, L. Luo, H. L. Huang and J. Zhang, *Colloids Surf., A*, 2014, **461**, 126–132.

56 Y. L. Wang, P. F. Hou, Z. Wang and P. Kang, *ChemPhysChem*, 2017, **18**, 3142–3147.